Artesunate synergistically promotes sorafenib-induced apoptosis and ferroptosis in non-Hodgkin lymphoma cells through inhibition of the STAT3 pathway

YINGYING CHEN[1,2], HUAN TAO[1], FUJUE WANG[3], PENGQIANG WU[4], JIE GAO[5], XUE ZHANG[1], ZHENGCANG HE[1], ZHENCANG ZHOU[1] and YONGQIAN JIA[1]

[1]Department of Hematology and Institute of Hematology, West China Hospital, Sichuan University; [2]Department of Oncology, Sichuan Cancer Hospital, Chengdu, Sichuan 610041; [3]Department of Hematology, The First Affiliated Hospital of University of South China, Hengyang, Hunan 421001; [4]Department of Hematology, The First Affiliated Hospital of Southwest Medical University, Luzhou, Sichuan 646000; [5]Department of Hematology, Shanghai General Hospital, Shanghai Jiao Tong University, Shanghai 200940, P.R. China

Received September 14, 2022; Accepted February 16, 2023

DOI: 10.3892/or.2023.8584

Abstract. Despite the development of advanced therapies, the prognosis of non-Hodgkin lymphoma (NHL) remains unsatisfactory due to refractory and relapsed cases. Artesunate (ART) and sorafenib (SOR) both exert potential antitumor activity in lymphoma. The present study aimed to investigate whether ART and SOR produce synergistic anti-lymphoma effects, and to determine the potential underlying mechanisms. Cell viability assay, flow cytometry, malondialdehyde assay, GSH assay and western blotting were performed to evaluate cell viability, and changes in apoptosis, autophagic vacuoles, reactive oxygen species, mitochondrial membrane potential, lipid peroxidation and protein expression. The results demonstrated that ART and SOR synergistically inhibited the viability of NHL cells. ART and SOR also synergistically induced apoptosis, and markedly increased the expression levels of cleaved caspase-3 and poly (ADP-ribose) polymerase. Mechanistically, ART and SOR synergistically induced autophagy, and rapamycin enhanced the ART- or SOR-induced inhibition of cell viability. Furthermore, it was demonstrated that ferroptosis promoted ART- and SOR-induced cell death through increasing lipid peroxides. Erastin enhanced the inhibitory effects of ART and SOR on cell viability, whereas ferrostatin-1 reduced the ART- and SOR-induced apoptosis of SU-DHL4 cells. Further studies revealed that signal transducer and activator of transcription 3 (STAT3) contributed to ferroptosis induced by ART and SOR in NHL cells, and genetic inhibition of STAT3 promoted ART/SOR-induced ferroptosis and apoptosis, concomitantly reducing the expression levels of glutathione peroxidase 4 and myeloid cell leukemia-1. Moreover, the combined treatment of ART and SOR exerted inhibitory effects on tumor growth, as well as antiangiogenic activity, resulting in the inhibition of CD31 expression in a xenograft model. Collectively, these findings indicated that ART acted synergistically with SOR to inhibit cell viability, and to induce apoptosis and ferroptosis through regulating the STAT3 pathway in NHL. Notably, ART and SOR may act as potential therapeutic agents for the treatment of lymphoma.

Introduction

Non-Hodgkin lymphoma (NHL) is a type of cancer of the lymphatic system that can be divided into B-, T- or natural killer-cell NHL (1). Among the types of NHL, B-cell NHL affects up to ~85% of all patients, and diffuse large B-cell lymphoma (DLBCL) is the most prevalent and aggressive subtype. Moreover, T-cell lymphoma represents only 10-15% of cases (2). Compared with Hodgkin lymphoma (HL), NHL is more complex due to different cell origins, diverse biological characteristics and clinical pathology. Notably, patients with NHL have a poor prognosis (3). According to the systematic analysis for the Global Burden of Diseases Study 2017, ~488,000 patients were newly diagnosed with NHL (4), and 248,000 deaths occurred worldwide (5). In 2016, it was estimated that 68,500 new patients were diagnosed with NHL and 37,600 NHL-related deaths occurred in China (6). Treatment options, including chemotherapeutic agents (rituximab, cyclophosphamide, adriamycin, vincristine and prednisone), targeted therapy, stem cell transplantation and chimeric antigen receptor T-cell therapy, have improved the clinical outcomes and prognosis of patients with NHL (3). However, relapse or refractory disease leads to unsatisfactory results, particularly in certain subtypes of lymphoma. In primary central nervous system (CNS) lymphoma, a rare and aggressive subtype of

Correspondence to: Professor Yongqian Jia, Department of Hematology and Institute of Hematology, West China Hospital, Sichuan University, 37 Guo Xue Xiang Street, Chengdu, Sichuan 610041, P.R. China
E-mail: jia_yq@scu.edu.cn

Key words: artesunate, sorafenib, ferroptosis, signal transducer and activator of transcription 3, non-Hodgkin lymphoma

NHL, the blood-brain barrier (BBB) is a major obstacle for successful clinical treatment. Therefore, further investigations into novel therapeutic agents are required.

Artesunate (ART), a semisynthetic compound of artemisinin, has been recommended by the World Health Organization for the front-line treatment of malaria, particularly cerebral malaria (7,8). Notably, ART may be a potential option for the treatment of diseases affecting the CNS. A previous study demonstrated that ART suppresses glioma through the regulation of mevalonate metabolism and the promotion of cell senescence (9). Moreover, previous studies have revealed that ART exerts profound anticancer biological activities in various types of solid tumors and hematological malignancies, both *in vitro* and *in vivo* (10,11). ART can also inhibit tumor growth via endoplasmic reticulum (ER) stress and unfolded protein response (UPR) pathways in lymphoma *in vitro* and *in vivo* (12). Studies have also revealed that ART can induce ferroptosis in glioblastoma and renal cell carcinoma cells (13,14). In addition, ART has been administered for the treatment of numerous types of cancer in clinical trials, including lung (15), cervical (16), breast (17) and colorectal cancer (18). These results suggested that ART might exhibit potential as an anticancer therapy due to the associated biological activity and tolerability.

Sorafenib (SOR) is a multikinase molecular inhibitor, which exerts anticancer activities through inhibiting cell proliferation, inducing apoptosis and inhibiting tumor angiogenesis in various cancer models, including in hepatocellular carcinoma (19), leukemia (20) and lymphoma (21). SOR has been shown to synergistically induce apoptosis when combined with vorinostat via downregulation of the anti-apoptotic protein, myeloid cell leukemia-1 (MCL-1), in T-cell lymphoma (22). Moreover, SOR exerts antitumor effects on tumors of CNS (23), thus indicating that SOR, similar to ART, may be a candidate for the treatment of CNS disorders.

The results of our previous study demonstrated that ART could induce ferroptosis in DLBCL cells (24). Notably, ART promotes antitumor effects via numerous mechanisms (25); however, monotherapy exhibits limited efficacy, and combined treatment is recommended for the treatment of lymphoma. ART exhibits potential for the treatment of cancer and other diseases (26), including diseases of the CNS, due to a higher concentration of ART in the brain (27), which indicates a high BBB permeability. SOR also exhibits potential in the treatment of diseases of the CNS (28). Thus, the present study aimed to investigate the combined effects of ART and SOR, and to explore the associated mechanisms in NHL cells. These treatments may exhibit potential as effective strategies in the treatment of NHL, and this study may provide a novel theoretical basis for the treatment of CNS-related diseases in the future.

Materials and methods

Reagents. ART (cat. no. MB7316), SOR (cat. no. MB1666), and Cell Counting Kit-8 (CCK-8; cat. no. MA0218) were purchased from Dalian Meilun Biology Technology Co., Ltd. Erastin (Era; cat. no. HY-15763), ferrostatin-1 (Fer; cat. no. HY-100579) and rapamycin (Rapa; cat. no. HY-10219) were purchased from MedChemExpress. Monodansylcadaverine (MDC; cat.no. 30432) was purchased from Sigma-Aldrich; Merck KGaA. BODIPY-C11 581/591 (cat. no. RM02821) was purchased from ABclonal Biotech Co., Ltd. According to the manufacturers' protocols, products (ART, SOR, Era, Fer, Rapa, MDC and BODIPY-C11) were dissolved in DMSO and stored at -20˚C. Plasmids (pLKO.1-Neo, cat. no. SHC001, originally from Sigma-Aldrich; Merck KGaA; psPAX2, cat. no. 12260, originally from Addgene, Inc.; and pMD2.G, cat. no. 12259, originally from Addgene, Inc.) were obtained from the Institute of Hematology, West China Hospital, Sichuan University (Chengdu, China). The short hairpin RNAs (shRNAs) [shRNA (sh)-signal transducer and activator of transcription 3 (STAT3), 5'-CCGGGCACAATCTAC GAAGAATCAACTCGAGTTGATTCTTCGTAGATTGTG CTTTTTG-3'; non-targeting negative control, 5'-CCGGCA ACAAGATGAAGAGCACCAACTCGAGTTGGTGCTCTT CATCTTGTTGTTTTTG-3'] were synthesized by TsingKe Biological Technology.

Cell culture. Human lymphoma cell lines (U2932, cat. no. ACC 633; SU-DHL4, cat. no. CRL-2957; SU-DHL6, cat. no. CRL-2959; and Jurkat, cat. no. CRL-2898), a mouse lymphoma cell line (EL4, cat. no. TIB-39) and 293T (cat. no. CRL-11268) cells were obtained from the Institute of Hematology, West China Hospital, Sichuan University, and provided by Professor Yongqian Jia. U2932 was originally from the Leibniz Institute DSMZ and the other cell lines were originally from the ATCC. U2932, SU-DHL4 and SU-DHL6 cells were cultured in RPMI-1640 medium (cat. no. SH30809; HyClone; Cytiva) supplemented with 20% FBS (cat. no. 900-108; Gemini Bio Products); Jurkat and EL4 cells were cultured in RPMI-1640 medium supplemented with 10% FBS; and 293T cells were cultured in DMEM/high glucose medium (cat. no. SH30243.01; HyClone; Cytiva) supplemented with 10% FBS. All cells were treated with 1% penicillin/streptomycin (cat. no. SV30010; HyClone; Cytiva) and maintained at 37˚C in an atmosphere containing 5% CO_2. U2932, SU-DHL4 and SU-DHL6 are B-cell lymphoma cell lines, and Jurkat is T-cell lymphoma cell line. Not all lymphoma cell lines were used in each experiment.

Antibodies. The primary antibodies used were as follows: Anti-cleaved poly (ADP-ribose) polymerase (PARP; cat. no. A5034; 1:1,000), anti-p62 (cat. no. A5180; 1:1,000), anti-LC3B-I/II (cat. no. A5202; 1:1,000), anti-ERK1/2 (ERK; cat. no. A5029; 1:1,000), anti-phosphorylated (p)-ERK (cat. no. A5036; 1:1,000), anti-MEK1/2 (MEK; cat. no. A5606; 1:1,000), anti-p-MEK (cat. no. A5191; 1:1,000), anti-glutathione peroxidase 4 (GPX4; cat. no. A5569; 1:1,000), anti-ATG5 (cat. no. A5745; 1:1,000) and anti-ferritin heavy chain 1 (FTH1; cat. no. A5654; 1:1,000) (all from Bimake). In addition, anti-STAT3 (cat. no. 4904; 1:2,000), anti-p-STAT3 (Tyr727; cat. no. 9134; 1:1000), anti-AKT (cat. no. 2938; 1:1,000), anti-p-AKT (cat. no. 9018; 1:1,000) and anti-Bcl-XL (cat. no. 2764; 1:1,000) were purchased from Cell Signaling Technology, Inc. Anti-cleaved caspase-3 (cat. no. WL02117; 1:500), P70S6K (cat. no. WL03839; 1:500) and anti-p-P70S6K (cat. no. WL04213; 1:500) antibodies were purchased from Wanleibio Co., Ltd. Anti-CD31 (cat. no. GB11063; 1:500) was purchased from Wuhan Servicebio Technology Co., Ltd., and anti-β-actin (cat. no. TA-09; 1:2,000), HRP-conjugated anti-rabbit IgG (cat. no. ZB-2306) and

HRP-conjugated anti-mouse IgG (cat. no. ZB-2305) secondary antibodies were purchased from OriGene Technologies, Inc.

Cell viability assay. Cells ($1x10^4$/well; U2932, SU-DHL4, SU-DHL6 and Jurkat) were inoculated in a 96-well plate with 100 μl medium, and were treated with ART (1, 2, 3, 4 and 5 μM for SU-DHL4 and SU-DHL6; 1, 5, 10, 15 and 20 μM for U2932 and Jurkat,) and SOR (2.5, 5, 10, 15 and 20 μM) at different concentrations for 48 h at 37˚C, or combined with or without Rapa (5 μM)/Era (1 μM)/Fer (5 μM) for 24 h at 37˚C. Subsequently, CCK-8 (10 μl) was added to each well and incubated for 2 h at 37˚C. Subsequently, the optical density (OD) of each well was detected at a wavelength of 450 nm (SpectraMax 190; Molecular Devices, LLC). Cell viability was calculated using the following equation: Cell viability (%)=[($OD_{treated}$-OD_{blank})/($OD_{control}$-OD_{blank})] x100. The combination indices were analyzed using CompuSyn software (v1.0; ComboSyn, Inc.).

Apoptosis analysis. Cells, cultured in a 6-well plate ($1x10^5$/well; U2932, SU-DHL4, SU-DHL6 and Jurkat), were harvested and detected using the Annexin V-647/PI Cell Apoptosis Detection kit (cat. no. Y6026; Suzhou Yuheng Biotechnology Co., Ltd). According to the manufacturer's instructions, each sample was resuspended in 300 μl binding buffer with 2 μl Annexin V and 1 μl PI, and then incubated for 15 min at room temperature in the dark. Sample acquisition and analysis were performed using a flow cytometer (Cytoflex; Beckman Coulter, Inc.) and FlowJo software 10.0 (FlowJo LLC).

Reactive oxygen species (ROS) assay. Cells, cultured in a 6-well plate ($1x10^5$/well; U2932, SU-DHL4 and Jurkat), were collected and stained with 5 μM diluted dichlorodihydrofluorescein diacetate (cat. no. S0033S; Beyotime Institute of Biotechnology), followed by incubation for 30 min in the dark at 37˚C according to the manufacturer's instructions. Cell acquisition and analysis were performed using a flow cytometer, as aforementioned.

JC-1 assay. Mitochondrial membrane potential (MMP) was measured using a JC-1 Kit (cat. no. M8650; Beijing Solarbio Science & Technology Co., Ltd.). According to the manufacturer's instructions, cells, cultured in a 6-well plate ($1x10^5$/well; U2932, SU-DHL4 and Jurkat), were stained with JC-1 dye and incubated for 30 min in the dark at 37˚C. The fluorescence intensity was measured and analyzed using a flow cytometer, as aforementioned.

MDC staining assay. Autophagic vacuoles in cells were detected using MDC staining. Briefly, cells, cultured in a 6-well plate ($1x10^5$/well; U2932, SU-DHL4 and Jurkat), were collected and stained with 50 μM MDC in 1X PBS at 37˚C for 30 min. MDC-stained cells were detected and analyzed using a flow cytometer, as aforementioned.

Lipid peroxidation assay. Changes in lipid peroxidation were detected using BODIPY-C11 581/591. Cells, cultured in a 6-well plate ($1x10^5$/well; U2932, SU-DHL4 and Jurkat), were harvested, washed, stained with 50 μM C11-BODIPY and incubated at 37˚C for 1 h in the dark. Subsequently, cells were detected and the mean fluorescence intensity was quantified using a flow cytometer, as aforementioned.

Malondialdehyde (MDA) assay. The relative levels of MDA were qualitatively detected using a Lipid Peroxidation MDA Assay kit (cat. no. S0131S; Beyotime Institute of Biotechnology) according to the manufacturer's protocol. Briefly, proteins were extracted from U2932 and Jurkat cells ($1x10^7$) using lysis buffer, and supernatants were mixed with TBA detection solution, heated for 15 min in a boiling water bath, cooled to room temperature and centrifuged (1,000 x g for 10 min at room temperature). Subsequently, the supernatants were transferred to a 96-well plate. The optical density was detected at a wavelength of 532 nm, and MDA content was calculated according to a standard curve and normalized to total protein levels.

GSH assay. The levels of GSH were evaluated using a GSH assay kit (cat. no. BC1175; Beijing Solarbio Science & Technology Co., Ltd) according to the manufacturer's protocol. Briefly, cells ($1x10^7$; U2932 and Jurkat) were collected and homogenized in solution I, followed by centrifugation. The supernatants were added into a 96-well plate, then incubated at room temperature for 2 min with solution II and solution III, along with standards. The optical density was detected at a wavelength of 412 nm (SpectraMax 190; Molecular Devices, LLC). GSH levels were calculated according to the standard curve and normalized to total protein levels.

Western blot analysis. Cells were collected and lysed in RIPA lysis buffer (cat. no. HY-K1001; MedChemExpress) supplemented with protease inhibitors (cat. no. P1260; Beijing Solarbio Science & Technology Co., Ltd.) and PMSF (cat. no. P0100; Beijing Solarbio Science & Technology Co., Ltd) on ice for 30 min. Protein concentration was measured using a BCA protein assay kit (cat. no. CW0014S; CoWin Biosciences). Protein samples (20-30 μg/lane) were separated by SDS-PAGE on 8-12% gels and transferred onto nitrocellulose membranes (cat. no. BSP0161; Pall Life Sciences). Membranes were subsequently blocked with 5% (w/v) skimmed milk at room temperature for 1 h and were incubated with primary antibodies at different dilutions according to the manufacturers' protocols overnight at 4˚C. After primary antibody incubation, the membranes were washed with 1X TBS-0.1% Tween-20 three times and were incubated with HRP-conjugated secondary antibodies (1:5,000) at room temperature for 1 h. After further washing, signals were visualized using an Ultra High Sensitivity ECL kit (cat. no. HY-K1005; MedChemExpress) on a Tanon 5200 chemiluminescence image analysis system (Tanon Science and Technology Co., Ltd).

Immunohistochemical (IHC) staining assay. Tumor tissues and organs were extracted from mice and fixed in 4% paraformaldehyde for 24 h at room temperature. IHC staining was performed using an immunohistochemistry kit (cat. no. G1215; Wuhan Servicebio Technology Co., Ltd.). Briefly, after dehydrating in a gradient alcohol series and permeabilizing with xylene, tissues were embedded in paraffin and cut into 5-μm sections. After dewaxing and hydration, organ tissue sections were stained using a hematoxylin/eosin staining kit

(cat. no. G1120; Beijing Solarbio Science & Technology Co., Ltd.). The tumor tissue sections were also dewaxed and rehydrated, and antigen retrieval was performed in boiled saline sodium citrate buffer for 10 min. The tissue sections were then blocked with 5% FBS at 37˚C for 15 min and stained with an anti-CD31 antibody (1:1,000) overnight at 4˚C. Subsequently, sections were detected using an IHC detection kit; the slides were incubated with secondary antibody (1:200) at 37˚C for 1 h, and processed with 3,3'-diaminobenzidine. Slides were observed under an optical microscope (Olympus Corporation) and analyzed using Image-Pro plus software (version 6.0; Media Cybernetics, Inc.)

RNA interference. According to the manufacturer's protocol, briefly, 293T cells were seeded in 10 cm dishes at a cell density of 60-70% and cultured overnight. The medium was replaced 6 h before transfection. Then pLKO.1-shRNA (10 μg), psPAX2 (7.5 μg) and pMD2.G (2.5 μg) plasmids, mixed with $CaCl_2$ (2 M; 62.5 μl; cat. no.C4901; Merck KGaA) and HBSS (2X HBSS; 500 μl; cat. no. 14065056; Thermo Fisher Scientific, Inc.) were co-transfected into 293T cells for 48 h using calcium phosphate co-precipitation at 37˚C. Viral supernatants were centrifuged at 1,000 x g for 10 min at 4˚C, filtered through a 0.45-μm filter. For infection, U2932 and SU-DHL4 cells ($2x10^5$/well) were seeded in a 6-well plate overnight and 1 ml of viral supernatant was added, then cells were cultured at 37˚C for 48 h. Next cells were selected with 1 μg/ml puromycin (cat. no. P8230; Beijing Solarbio Science & Technology Co., Ltd.). Infection efficiency was evaluated by western blotting. The concentration of puromycin used for maintenance was also 1 μg/ml.

Xenograft model analysis. To establish lymphoma xenograft models, a total of 20 female C57/BL/6 mice (weight, 20±2 g; age, 6-8 weeks) were purchased from Beijing Huafukang Biotechnology Co., Ltd. Mice were maintained in the West China Animal Experiment Center of Sichuan University. All mice had free access to food and water, and were maintained in stress-free, hygienic and animal-friendly conditions (temperature, 22˚C; humidity, 60%) under a 12-h light/dark cycle. All experimental procedures were approved by the Institutional Animal Care and Use Committee of Sichuan University (ethics approval no. 20211284A). Mice were injected subcutaneously with $5x10^5$ EL4 cells resuspended in 100 μl serum-free medium (n=5 mice/group). Tumor size was measured using electronic digital calipers, and the tumor volume (mm^3) was calculated as (length x $width^2$)/2. When the tumor volume reached 50-100 mm^3 after 5 days, mice were randomly divided into four groups and administered normal saline (NS, the control), ART (90 mg/kg), SOR (30 mg/kg) or the combined treatment of both ART and SOR (ART 90 mg/kg and SOR 30 mg/kg). Drugs were injected intraperitoneally every day until tumors reached 2 cm in diameter or had ulcerated, and mice were euthanized using cervical dislocation. Tumor tissues, livers and spleens were extracted from mice. Death of the mice was verified by cessation of heartbeat and breathing. The duration of the animal experiment was 2 weeks and no mice died during the experiment. The body weight, fur condition and general survival status were observed and recorded daily.

Statistical analysis. Data are presented as the mean ± standard deviation of three independent experiments. GraphPad Prism 8 (Dotmatics) was used for statistical analysis. A one-way ANOVA with Tukey's post hoc test was used for multi-group comparisons. $P<0.05$ was considered to indicate a statistically significant difference.

Results

ART and SOR synergistically inhibit the viability of NHL cells. To investigate the inhibitory effects of ART and SOR on lymphoma cell lines, the cells were treated with ART and SOR at different concentrations for 48 h. As shown in Fig. 1A and B, cell viability decreased in a dose-dependent manner when exposed to ART or SOR in U2932, SU-DHL4, SU-DHL6 and Jurkat cells. Subsequently, the present study aimed to examine whether ART and SOR exhibited synergistic effects on NHL cells. As shown in Fig. 1C, lymphoma cells treated with a combination of ART and SOR displayed a significant reduction in cell viability compared with that in groups treated with either ART or SOR alone. In addition, the combination indices were <1 in U2932 and Jurkat cells, which revealed the synergistic inhibitory effect of ART and SOR on the viability of NHL cells (Fig. S1A).

ART facilitates the SOR-induced apoptosis of NHL cells. To further determine the mechanism underlying the synergistic anti-lymphoma effects of ART and SOR, cell apoptosis induced by ART and SOR was assessed using flow cytometry. As shown in Fig. 2A, ART or SOR treatment induced the early and late apoptosis of lymphoma cells, but this was not obvious. Moreover, the combined treatment of ART and SOR significantly promoted the apoptosis of NHL cells compared with ART or SOR treatment alone. Notably, western blot analysis was performed to further verify these results. As shown in Fig. 2B, the expression levels of cleaved caspase-3 and PARP were increased, whereas Bcl-XL and MCL-1 expression levels were markedly decreased in the combined treatment group compared with those in the groups treated with either ART or SOR alone. These findings suggested that ART promoted SOR-induced apoptosis in NHL cells.

ART and SOR synergistically inhibit AKT and MEK/ERK pathways in NHL cells. The results of a previous study demonstrated that ART inhibits tumor cell proliferation via regulation of the AKT signaling pathway (29). Subsequently, whether the combined treatment of ART and SOR affected AKT and MEK/ERK pathways was assessed in U2932, SU-DHL4 and Jurkat cells. The results of western blot analysis demonstrated that the protein expression levels of p-AKT, p-P70S6K, p-MEK and p-ERK were reduced following ART or SOR treatment alone; however, these reductions were minor. Notably, the expression levels of the aforementioned proteins were more markedly reduced following the combined treatment of ART and SOR in lymphoma cells (Fig. 3). These results suggested that the combined treatment of ART and SOR exerted inhibitory effects on AKT and MEK/ERK pathways in NHL cells.

ART and SOR induce autophagy in NHL cells. The results of our previous study demonstrated that ART induced autophagy

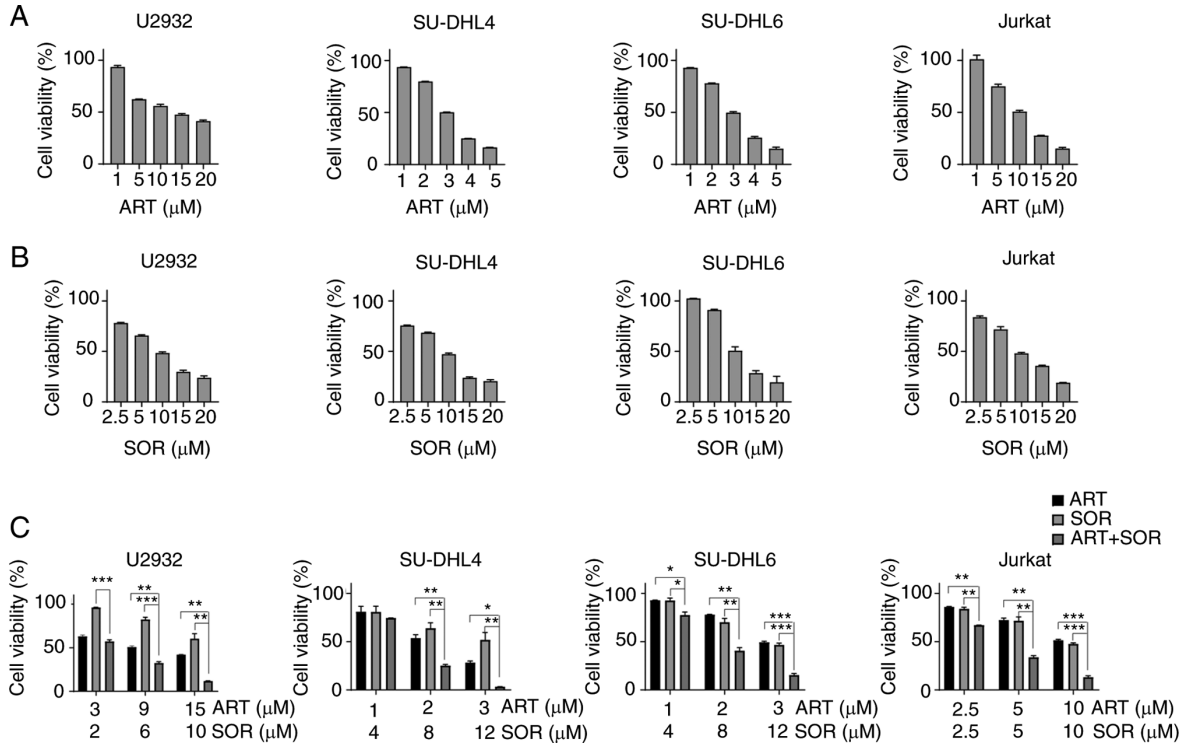

Figure 1. ART and SOR inhibit the viability NHL cells. NHL cells were treated with various concentrations of (A) ART or (B) SOR for 48 h. (C) Cells were treated with distinct concentrations of ART and SOR, alone or combination, for 48 h. Cell viability was measured by Cell Counting Kit-8 assay. Data are presented as the mean ± SD (n=3). *P<0.05, **P<0.01, ***P<0.001. ART, artesunate; NHL, non-Hodgkin lymphoma; SOR, sorafenib.

in DLBCL cell lines (29). Subsequently, whether the combined treatment of ART and SOR synergistically induced autophagy in lymphoma cells was investigated in the present study. As shown in Fig. 4A, the expression levels of LC3B-I/II and ATG5 were increased, whereas those of p62 were decreased following the combined treatment of ART and SOR compared with those in groups treated with ART or SOR alone. In addition, the MDC staining assay was performed to detect the levels of acidic vesicular organelles (30) following exposure to ART and/or SOR treatment for 24 h. Consistent with the aforementioned results, the fluorescence intensity of MDC was increased following ART or SOR treatment, but this was not significant, and a greater increase was observed in the combined treatment group compared with that in groups treated with ART or SOR alone (Fig. 4B). Notably, Rapa, an inducer of autophagy, enhanced the inhibitory effects of ART or SOR on the viability of U2932, SU-DHL4 and Jurkat cells (Fig. 4C). These results indicated that the synergistic inhibition induced by ART and SOR partially involved autophagy in lymphoma cells.

ART and SOR induce ferroptosis in NHL cells. It has been reported that both ART and SOR are ferroptosis inducers (31). Thus, the present study aimed to investigate whether ART and SOR induced ferroptosis in lymphoma cells. As shown in Fig. 5A, the expression levels of GPX4 and FTH1 were decreased following exposure to ART or SOR alone; however, these reductions were minor. Notably, a more marked reduction in the expression levels of the aforementioned proteins was observed following treatment with ART and SOR in combination compared with those in groups treated with ART or SOR alone. Levels of lipid peroxidation were detected using BODIPY-C11, and the results demonstrated that the combined treatment of ART and SOR induced a higher production of lipid peroxidation than groups treated with ART or SOR alone (Fig. 5B and C). Moreover, the levels of ROS accumulation were markedly increased to various extents following ART or SOR treatment, and ROS generation was significantly higher in the combined treatment group compared with that in groups treated with ART or SOR alone (Fig. S1B and C). Notably, the contents of MDA were significantly higher following the combined administration of ART and SOR compared with that in groups treated with ART or SOR alone (Fig. S1D). However, the levels of GSH were significantly lower in the combined treatment group compared with those in groups treated with ART or SOR alone (Fig. S1E). In addition, MMP was decreased following exposure to ART or SOR in lymphoma cells, but this was not significant; notably, more monomers were detected, which indicated a lower ratio of JC-1 aggregates and monomers occurred in drug-treated cells. A markedly lower level of MMP was also observed in the combined treatment group compared with that in groups treated with ART or SOR alone (Fig. 5D).

To further investigate the role of ferroptosis induced by ART and SOR, cells were co-treated with or without a ferroptosis inducer or inhibitor. As shown in Fig. 6A, Era further inhibited cell viability following treatment with ART or SOR. Moreover, co-treatment with Era markedly increased the levels of apoptosis in ART- or SOR-treated cells (ART: 5 μM, SOR: 5 μM) (Fig. 6B). By contrast, ferrostatin-1 partially reduced apoptosis induced by ART or SOR (ART: 10 μM, SOR: 10 μM; higher concentration used to ensure effect) in

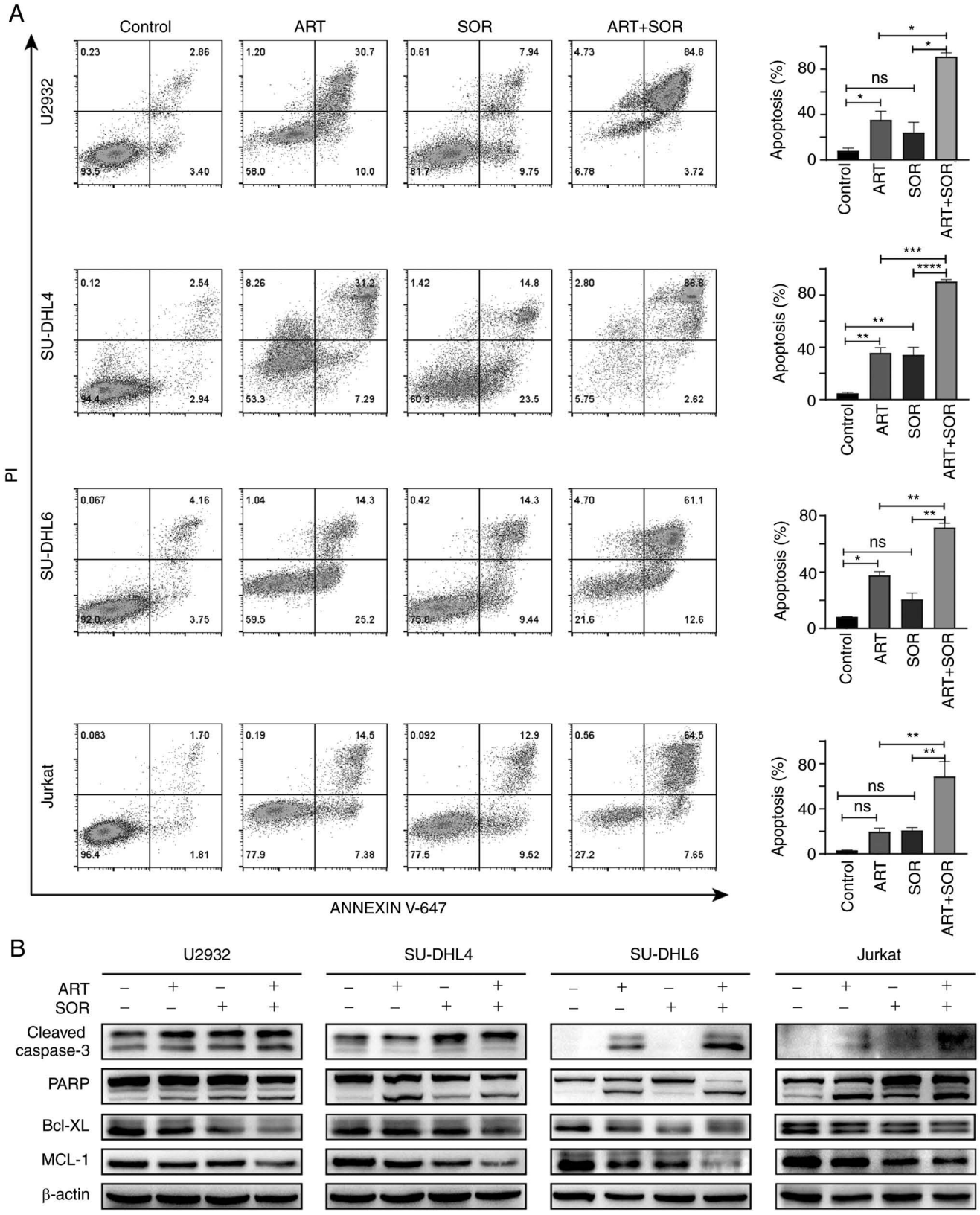

Figure 2. ART enhances the SOR-induced apoptosis of non-Hodgkin lymphoma cells. (A) Cells were treated with ART and SOR for 24 h. The apoptotic levels were detected using flow cytometry (left panel). The proportions of apoptotic cells are shown in histograms (right panel). (B) Expression levels of apoptosis-related proteins were measured using western blotting. The molecular weight of cleaved caspase-3 is 17/19, so two bands are presented. Cleaved PARP is presented in the lower level (the top band is the PARP). Data are presented as the mean ± SD (n=3). β-actin was used as a standard. *P<0.05, **P<0.01, ***P<0.001, ****P<0.0001. ART, artesunate; MCL-1, myeloid cell leukemia-1; PARP, poly (ADP-ribose) polymerase; SOR, sorafenib.

SU-DHL4 cells (Fig. 6C). These results suggested that ART and SOR synergistically induced ferroptosis, and ferroptosis may contribute to apoptosis induced by ART and SOR in NHL cells.

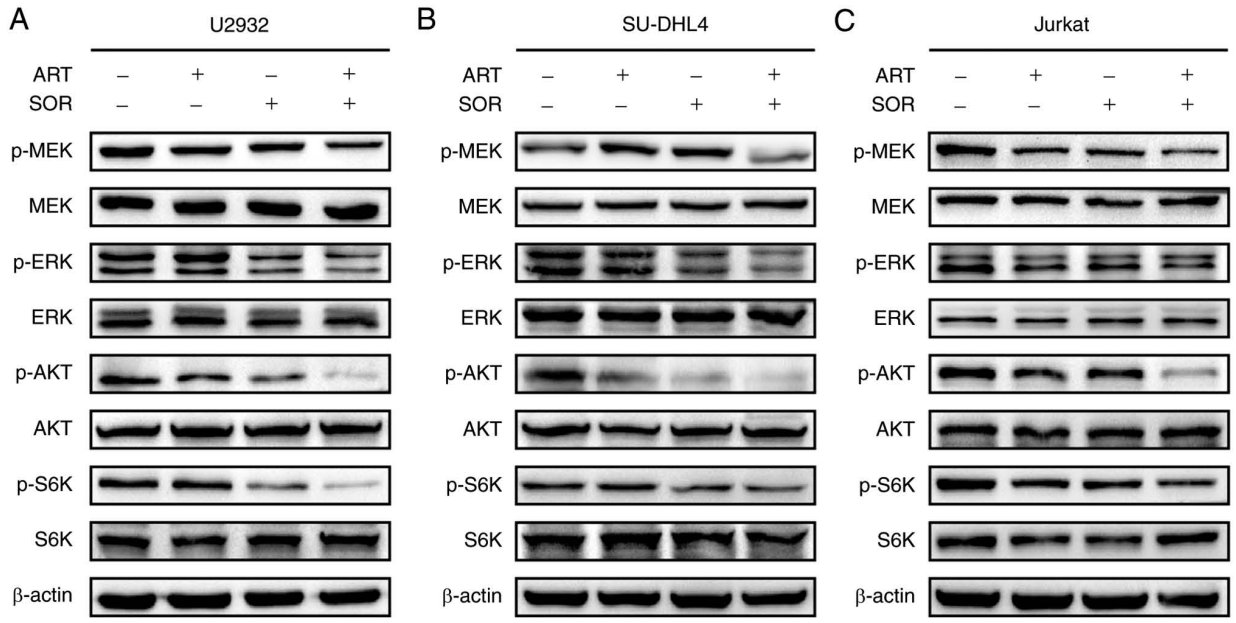

Figure 3. ART and SOR inhibit the AKT and MAPK pathways in NHL cells. Extracts from (A) U2932, (B) SU-DHL4 and (C) Jurkat NHL cells treated with ART (5 μM) and/or SOR (5 μM) for 24 h underwent western blotting to determine changes in the expression levels of proteins associated with the AKT and MAPK pathways. β-actin was used as a standard. ART, artesunate; NHL, non-Hodgkin lymphoma; p-, phosphorylated; S6K, P70S6K; SOR, sorafenib.

ART and SOR induce ferroptosis via regulation of STAT3 in NHL cells. The results of previous studies have demonstrated that STAT3 regulates ferroptosis (32,33). Therefore, whether STAT3 was involved in the inhibitory effects induced by a combination of ART and SOR was investigated in the present study. The results of the western blot analysis demonstrated that the combined treatment of ART and SOR inhibited p-STAT3 protein expression compared with that in groups treated with ART or SOR alone (Fig. 7A). Subsequently, to further validate the role of STAT3 in ART- and SOR-induced ferroptosis in lymphoma cells, the expression of STAT3 was inhibited using RNA interference (Fig. S1F), as previously described (29). As shown in Fig. 7B, the expression levels of MCL-1 and GPX4 were markedly decreased following ART or SOR treatment in cells transfected with sh-STAT3 compared with those in the sh-Control cells. In addition, the apoptotic rates induced by ART and SOR were higher in the sh-STAT3 groups than those in the sh-Control groups in SU-DHL4 cells, whereas there was no significant difference in apoptosis between cells treated with ART/SOR and the control group (Fig. 7C). Moreover, the production of lipid peroxidation was increased in cells treated with ART or SOR and transfected with sh-STAT3 compared with that in the sh-Control groups (Fig. 7D). Collectively, these results suggested that STAT3 regulated ART- and SOR-induced apoptosis and ferroptosis in lymphoma cells.

Combined treatment of ART and SOR inhibits tumor growth in vivo. Subsequently, the anti-lymphoma effects of ART and SOR were investigated *in vivo*. EL4 cells were subcutaneously injected into C57BL/6 mice. In Fig. S2, the *in vitro* results shown that ART/SOR could also inhibit cell viability, induce apoptosis, ROS and lipid peroxidation accumulation in EL4 cells. After the tumors were palpable, mice were randomly divided into four groups and treated intraperitoneally with NS (control), ART, SOR or ART + SOR. As shown in Fig. 8A and B, tumor growth was suppressed following ART and SOR administration. In addition, compared with groups treated with ART or SOR alone, tumor volumes in the ART + SOR treatment group were significantly reduced. Moreover, compared with that in groups treated with ART or SOR alone, the weight of tumors was also smaller in the combined treatment group (Fig. 8C). Consistent with the *in vitro* results, the expression levels of GPX4, FTH1 and p-STAT3 were reduced in the ART + SOR treatment group compared with those in the groups treated with ART or SOR alone (Fig. 8D). In addition, IHC staining was performed to measure the effect of ART and SOR on angiogenesis. Reduced CD31-positive areas were observed in the ART or SOR groups compared with those in the NS group. Moreover, ART + SOR exhibited a markedly synergistic effect on inhibiting tumor angiogenesis compared with either ART or SOR monotherapy (Fig. 8E and F). However, the body weights of mice did not change significantly among the four groups (Fig. 8G). Finally, the liver and spleen tissues were removed from the mice and stained with hematoxylin and eosin. There were no marked changes among the four groups, which indicated that the combination treatment did not lead to apparent toxicity (Fig. 8H). Hence, the results demonstrated that the combination of ART and SOR performed synergistic effects and was well tolerated *in vivo*.

Discussion

The results of the present study demonstrated that, in combination, ART and SOR synergistically exerted anti-lymphoma effects *in vitro* and *in vivo*. The combined treatment of ART and SOR synergistically suppressed cell viability, and induced cell apoptosis, autophagy and ferroptosis in NHL cells. In addition, STAT3 played an important role in ART/SOR-induced apoptosis and ferroptosis.

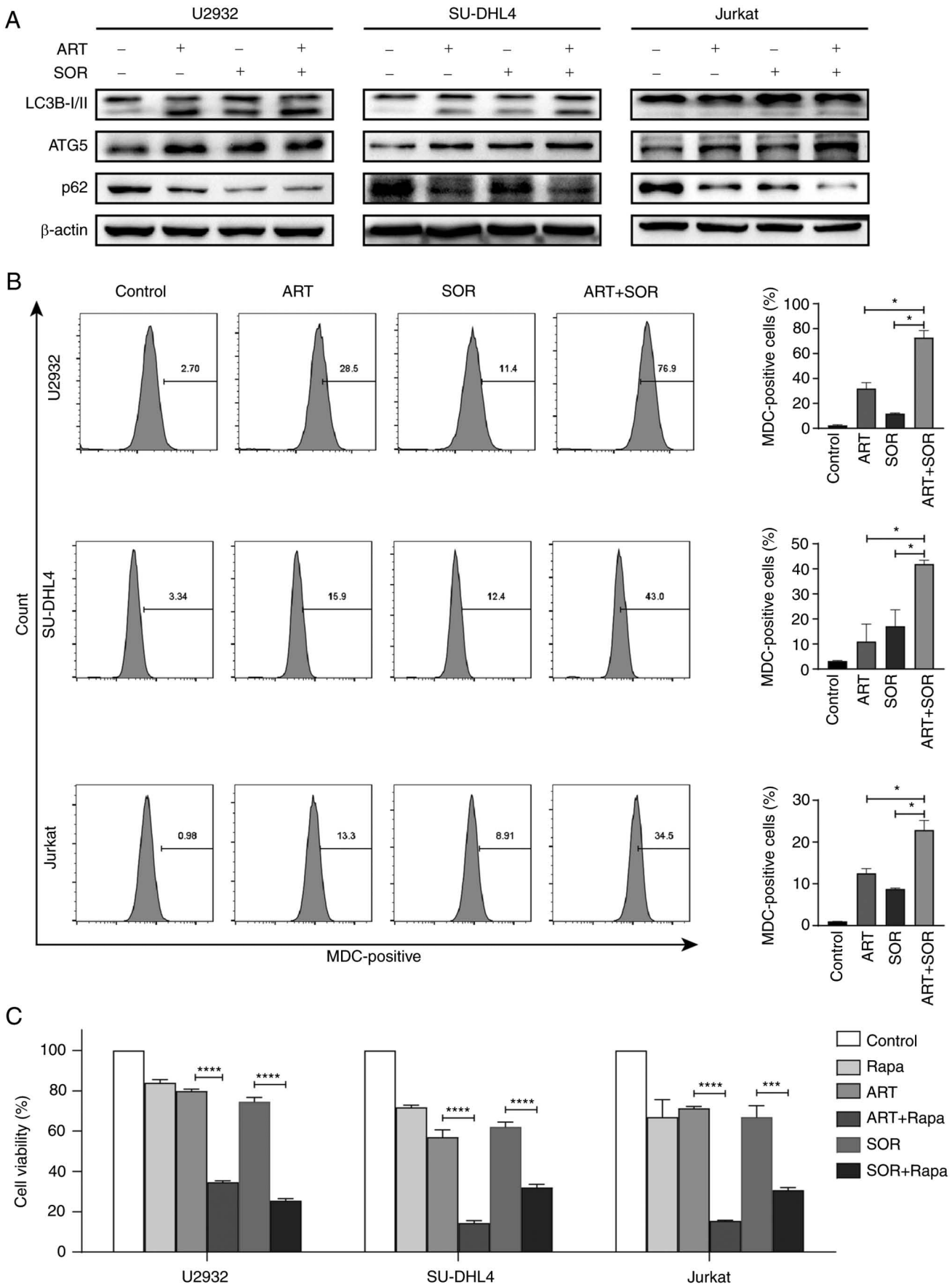

Figure 4. ART and SOR induce autophagy in non-Hodgkin lymphoma cells. (A) Western blotting was used to evaluate changes in autophagy-related proteins in cells treated with ART (5 μM) and/or SOR (5 μM) for 24 h. (B) After treatment with ART and/or SOR for 24 h, MDC staining was used to determine the changes in autophagy levels (left panel). The proportion of MDC-positive cells is shown in histograms (right panel). (C) Cells were co-treated with ART/SOR and Rapa (5 μM) for 24 h. Cell viability was measured by Cell Counting Kit-8 assay. Data are presented as the mean ± SD (n=3). β-actin was used as a standard. *P<0.05, ***P<0.001, ****P<0.0001. ART, artesunate; MDC, monodansylcadaverine; Rapa, rapamycin; SOR, sorafenib.

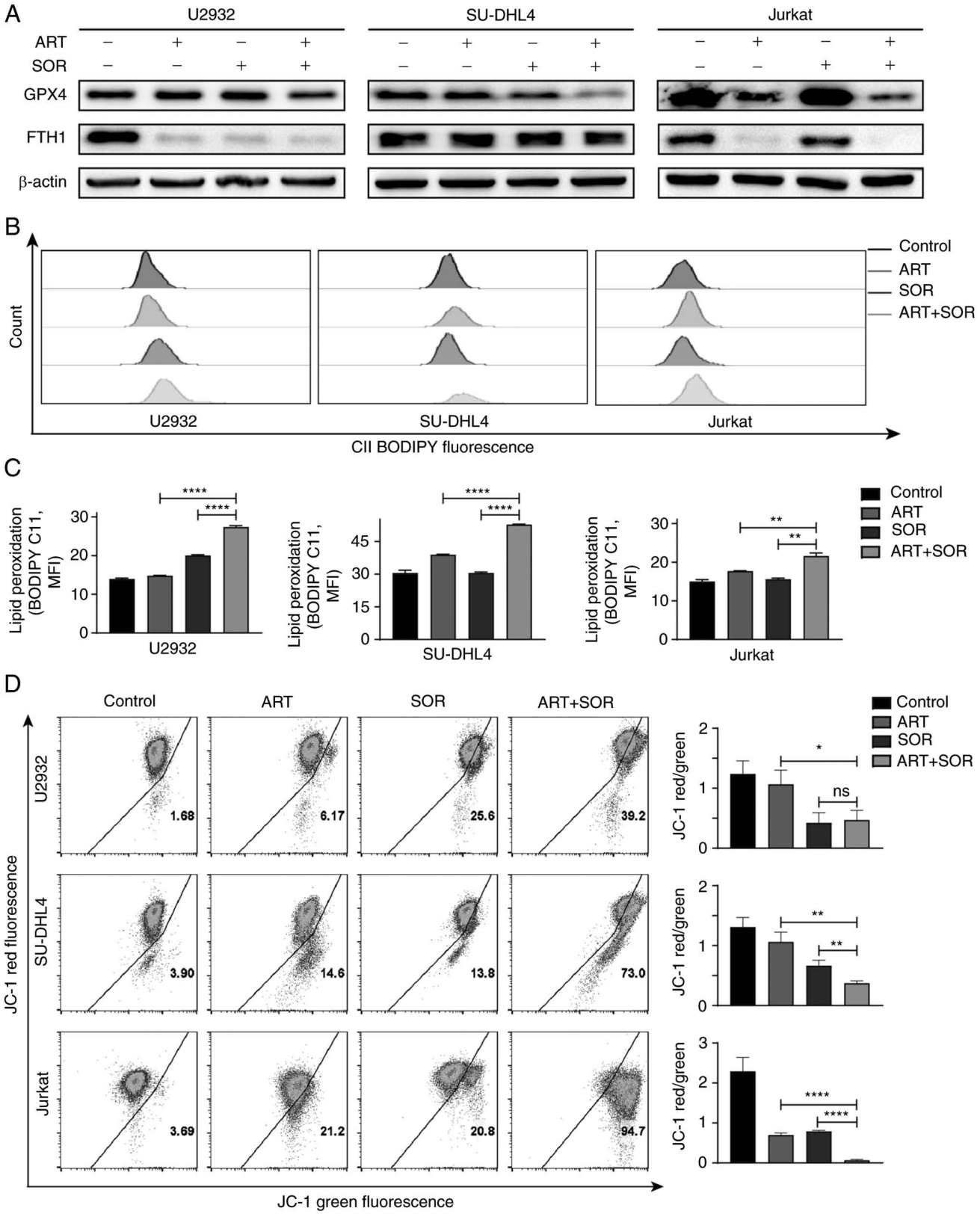

Figure 5. ART and SOR induce ferroptosis in non-Hodgkin lymphoma cells. (A) Western blotting was used to detect the expression levels of ferroptosis-related proteins in cells treated with ART (5 μM) and/or SOR (5 μM) for 24 h. (B and C) Lipid peroxidation levels in cells were analyzed using flow cytometry. (D) Mitochondrial membrane potential levels in cells were stained with JC-1 (5 μM) and analyzed by flow cytometry following ART and/or SOR treatment for 18 h. Data are presented as the mean ± SD (n=3). β-actin was used as a standard. *P<0.05, **P<0.01, ****P<0.0001. ART, artesunate; FTH1, ferritin heavy chain 1; GPX4, glutathione peroxidase 4; SOR, sorafenib; MFI, mean fluorescence intensity.

Furthermore, results of the *in vivo* analysis suggested that the combined treatment of ART and SOR synergistically delayed subcutaneous tumor growth and inhibited angiogenesis.

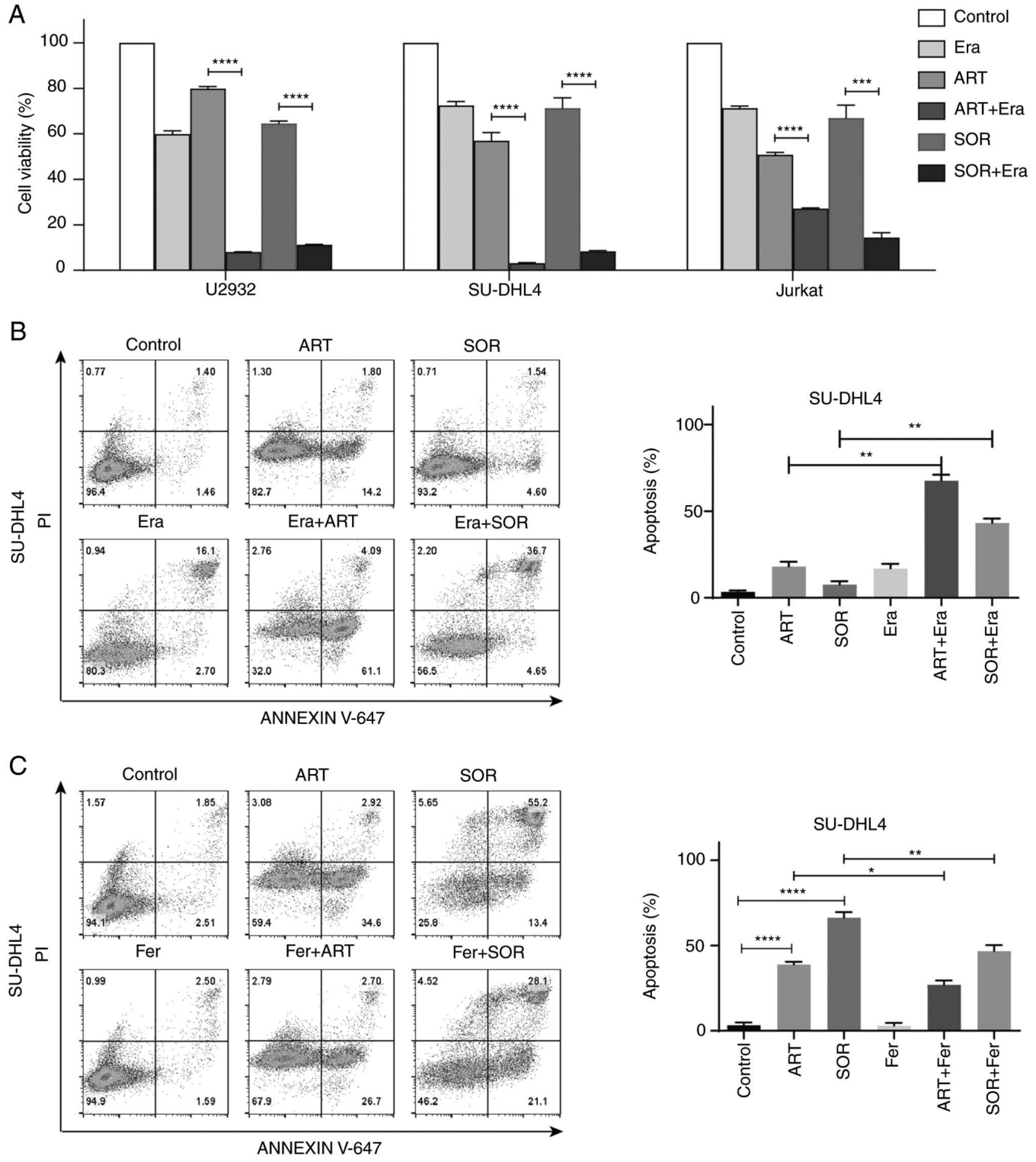

Figure 6. Ferroptosis facilitates ART/SOR-induced inhibition in non-Hodgkin lymphoma cells. (A) Cell viability following ART/SOR treatment of cells with or without Era (0.5 μM) for 24 h. (B) Cells were co-administered ART (5 μM)/SOR(5 μM) with or without Era (1 μM) for 24 h. Apoptosis was analyzed using flow cytometry. (C) Cells were co-administered ART (10 μM)/SOR (10 μM) with or without Fer (5 μM) for 24 h. Apoptosis was analyzed using flow cytometry. Data are presented as the mean ± SD (n=3). *P<0.05, **P<0.01, ***P<0.001, ****P<0.0001. ART, artesunate; Era, erastin; Fer, Ferrostatin-1; SOR, sorafenib.

Results of previous studies demonstrated that treatment with ART alone, or in combination with other clinical drugs, could exert potent antitumor activity in lymphoma *in vitro* and *in vivo* (34-36), and these results were also observed following treatment with SOR (37,38). In addition, SOR has been shown to suppress the MAPK/ERK and AKT pathways in lymphoma cells (39), and to synergize with Rapa to inhibit NHL cell proliferation (40). When in combination with perifosine, an AKT inhibitor, SOR can induce mitochondrial cell death via regulation of tribbles homologue 3 expression in HL (41). Notably, AKT and MAPK signaling pathways are activated in methotrexate-resistant primary CNS lymphoma-derived cells, highlighting that AKT

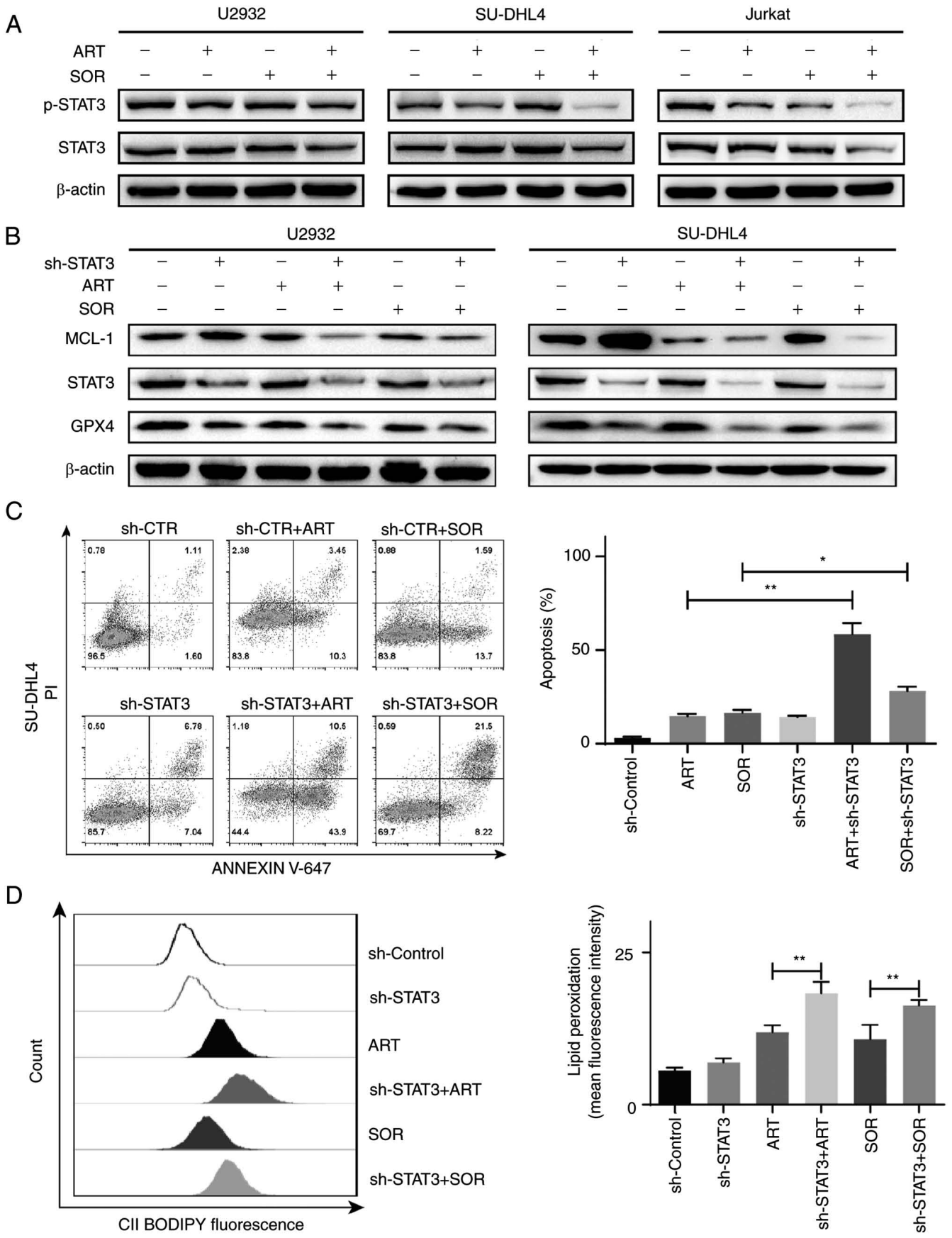

Figure 7. Role of STAT3 in ART/SOR-induced ferroptosis. (A) Western blotting was used to detect the protein expression levels of p-STAT3 in non-Hodgkin lymphoma cells following ART/SOR treatment. (B) Western blotting was used to detect the protein expression levels of apoptosis- and ferroptosis-related proteins in sh-STAT3- or sh-CTR cells following ART/SOR treatment. (C) Cells were treated with ART/SOR for 24 h. Flow cytometry was used to determine the levels of apoptosis. (D) Lipid peroxidation levels in cells were analyzed using flow cytometry. Data are presented as the mean ± SD (n=3). β-actin was used as a standard. *P<0.05, **P<0.01. ART, artesunate; CTR, control; GPX4, glutathione peroxidase 4; MCL-1, myeloid cell leukemia-1; p-, phosphorylated; sh, short hairpin; SOR, sorafenib; STAT3, signal transducer and activator of transcription 3.

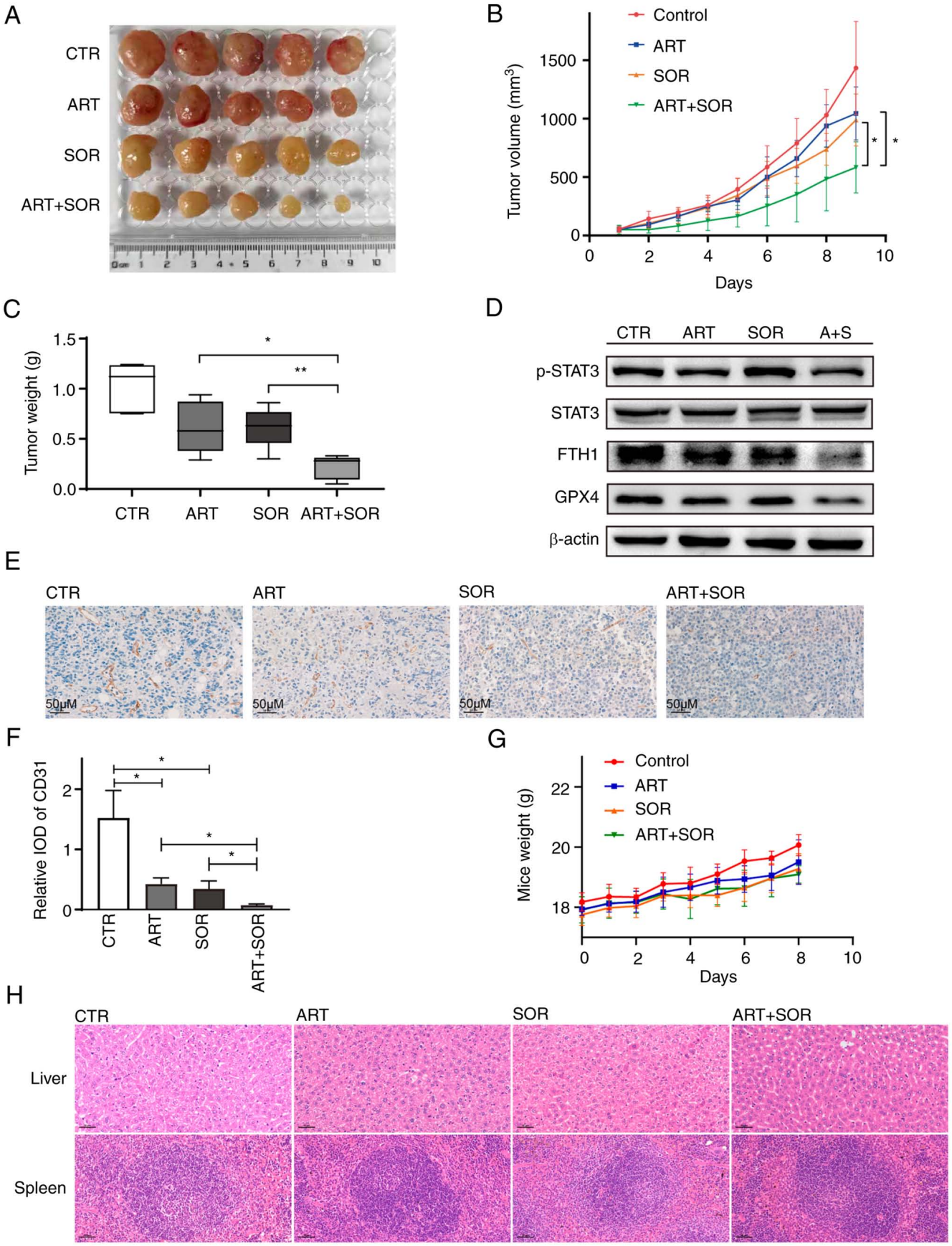

Figure 8. ART/SOR synergistically inhibit tumor growth *in vivo*. (A) Tumor tissues were isolated after 1 week of treatment. (B) Tumor volumes were calculated and plotted. (C) Tumor weight was calculated. (D) Western blotting was used to detect the protein expression levels in tumor tissues. (E and F) Expression of CD31 protein was evaluated in paraffin-embedded sections by immunohistochemical staining. (G) Body weight of mice. (H) Morphology of livers and spleens stained with hematoxylin and eosin. β-actin was used as a standard. Scale bars, 50 μm. *P<0.05, **P<0.01. ART, artesunate; CTR, control; FTH1, ferritin heavy chain 1; GPX4, glutathione peroxidase 4; p-, phosphorylated; SOR, sorafenib; STAT3, signal transducer and activator of transcription 3; IOD, integrated optical density.

or MAPK inhibitors may increase sensitivity to methotrexate in CNS lymphoma cells (42). The results of the present study also demonstrated that ART enhanced the inhibitory effects of SOR on the protein expression levels of p-AKT, p-MEK and p-ERK in lymphoma cells, indicating that the combined treatment of ART and SOR may exert anti-lymphoma effects on the AKT and MAPK signaling pathways.

The results of our previous study demonstrated that ART induced autophagy in DLBCL cells (29); however, it is inconclusive as to whether autophagy promotes or inhibits the antitumor effect induced by ART (43,44). Notably, autophagy also plays a paradoxical role in the anticancer effect of SOR (45,46). Moreover, results of the present study demonstrated that ART and SOR induced autophagy in lymphoma cells. In addition, Rapa, an autophagy inducer, enhanced ART- and SOR-induced inhibition of cell proliferation, which is consistent with the results of previous studies (40,44). These data indicated that ART and SOR induced autophagy, which may, at least partly, lead to synergistic inhibitory effects on lymphoma cells.

Ferroptosis is a novel form of non-apoptotic cell death. Previous studies have focused on the potential of ferroptosis induction in cancer therapy (47,48). Notably, both ART and SOR can induce ferroptosis in tumor cells (49). DLBCL cells have also been reported to be one of the most sensitive types of cells to ferroptosis in distinct tissues (50). The results of the present study demonstrated that ferroptosis induction occurred in ART- and SOR-treated cells via downregulation of GPX4 and FTH1 expression levels. Notably, iron accumulation, a marker of ferroptosis (51), which can further reflect the existence of ferroptosis, was not analyzed in the present study; however, the other main indicator of ferroptosis, lipid peroxidation, was increased following treatment with ART and SOR. Imidazole ketone erastin induces ferroptosis and inhibits lymphoma *in vitro* and *in vivo* (52). In addition, the present study demonstrated that Era enhanced ART- and SOR-induced inhibition of cell viability and promoted apoptosis. These results indicated that ferroptosis was involved in the ART- and SOR-induced synergistic inhibition of NHL cells. However, the association between ferroptosis and apoptosis is complex. Ferroptosis is different from, but seems to be linked to apoptosis. For example, inhibiting GPX4 activation can not only promote ferroptosis but also sensitize cells to apoptosis (53). Whereas Bcl-2, an anti-apoptotic protein, can be suppressed by ferroptosis inhibitors, which indicates that the role of Bcl-2 in apoptosis and ferroptosis remains elusive (54). The results of the present study demonstrated that Era promoted ART- or SOR-induced apoptosis, whereas ferrostatin-1 decreased the apoptosis induced by ART or SOR in SU-DHL4 cells. These findings indicated that there may be crosstalk between apoptosis and ferroptosis induced by ART and SOR. A previous study demonstrated that the UPR and ER stress induced by ferroptotic agents serve important roles between ferroptosis and apoptosis (55). Moreover, the results of a previous study revealed that ART can exert anti-lymphoma activity in malignant B cells via UPR and ER stress (12). Therefore, ferroptosis may promote apoptosis through the ER stress pathway in NHL cells treated with ART and SOR in combination. However, these results require further investigation.

STAT3 is an oncogenic driver in T- or B-cell lymphoma, and aberrant and constitutive activation of STAT3 predicts a poor prognosis (56,57). In addition, dimethyl fumarate treatment induces ferroptosis via inhibition of the NF-κB and STAT3 signaling pathways in DLBCL (33). The results of the present study also demonstrated that ART and SOR treatment downregulated the expression of p-STAT3, and STAT3 knockdown downregulated the protein expression levels of GPX4 and MCL-1 in U2932 and SU-DHL4 cells. These data suggested that the combination of ART and SOR induced ferroptosis and apoptosis in NHL cells via regulation of the STAT3 pathway. Although it has been demonstrated that STAT3 could regulate ferroptosis by mediating GPX4 expression, it remains unclear whether STAT3 transcriptionally or post-transcriptionally regulates GPX4 expression. Notably, the specific role of STAT3 in ferroptosis and apoptosis in lymphoma remains to be fully elucidated.

In conclusion, the results of the present study demonstrated that ART and SOR synergistically suppressed cell viability, and induced cell apoptosis, autophagy and ferroptosis *in vitro*. Notably, the STAT3 pathway exhibited a crucial association with apoptosis and ferroptosis induced by ART and SOR in NHL cells. In addition, ART and SOR synergistically inhibited tumor growth and decreased angiogenesis *in vivo*. These findings provide preclinical evidence for the potential application of ART and SOR in the treatment of NHL. Monotherapy is limited in the treatment of lymphoma; therefore, ART in combination with other chemical agents may exhibit potential in the treatment of NHL, as well as in the treatment of CNS lymphoma. Moreover, ferroptosis may also act as a potential target in the treatment of lymphoma or hematological malignancies in the future.

Acknowledgements

Not applicable.

Funding

No funding was received.

Availability of data and materials

The data used and/or analyzed during the current study are available from the corresponding author on reasonable request.

Authors' contributions

YJ and YC designed the study. YC performed the experiments, analyzed the data and drafted the manuscript. HT, FW, PW, JG, XZ, ZH and ZZ analyzed the data and designed the figures. YJ and YC confirm the authenticity of all the raw data. All authors read and approved the final manuscript.

Ethics approval and consent to participate

All experimental procedures were approved by the Institutional Animal Care and Use Committee of Sichuan University (ethics approval no. 20211284A).

Patient consent for publication

Not applicable.

Competing interests

The authors declare that they have no competing interests.

References

1. Swerdlow SH, Campo E, Pileri SA, Harris NL, Stein H, Siebert R, Advani R, Ghielmini M, Salles GA, Zelenetz AD and Jaffe ES: The 2016 revision of the world health organization classification of lymphoid neoplasms. Blood 127: 2375-2390, 2016.
2. Shankland KR, Armitage JO and Hancock BW: Non-hodgkin lymphoma. Lancet 380: 848-57, 2012.
3. Armitage JO, Gascoyne RD, Lunning MA and Cavalli F: Non-hodgkin lymphoma. Lancet 390: 298-310, 2017.
4. GBD 2017 Disease and Injury Incidence and Prevalence Collaborators: Global, regional, and national incidence, prevalence, and years lived with disability for 354 diseases and injuries for 195 countries and territories, 1990-2017: A systematic analysis for the global burden of disease study 2017. Lancet 392: 1789-1858, 2018.
5. GBD 2017 Causes of Death Collaborators: Global, regional, and national age-sex-specific mortality for 282 causes of death in 195 countries and territories, 1980-2017: A systematic analysis for the global burden of disease study 2017. Lancet 392: 1736-1788, 2018.
6. Liu W, Liu J, Song Y, Zeng X, Wang X, Mi L, Cai C, Wang L, Ma J and Zhu J; Union for China Leukemia Investigators of the Chinese Society of Clinical Oncology; Union for China Lymphoma Investigators of the Chinese Society of Clinical Oncology: Burden of lymphoma in China, 2006-2016: An analysis of the global burden of disease study 2016. J Hematol Oncol 12: 115, 2019.
7. White NJ: Qinghaosu (artemisinin): The price of success. Science 320: 330-334, 2008.
8. Song X, Wei W, Cheng W, Zhu H, Wang W, Dong H and Li J: Cerebral malaria induced by plasmodium falciparum: Clinical features, pathogenesis, diagnosis, and treatment. Front Cell Infect Microbiol 12: 939532, 2022.
9. Wei S, Liu L, Chen Z, Yin W, Liu Y, Ouyang Q, Zeng F, Nie Y and Chen T: Artesunate inhibits the mevalonate pathway and promotes glioma cell senescence. J Cell Mol Med 24: 276-284, 2020.
10. Raza A, Ghoshal A, Chockalingam S and Ghosh SS: Connexin-43 enhances tumor suppressing activity of artesunate via gap junction-dependent as well as independent pathways in human breast cancer cells. Sci Rep 7: 7580, 2017.
11. Ishikawa C, Senba M and Mori N: Evaluation of artesunate for the treatment of adult T-cell leukemia/lymphoma. Eur J Pharmacol 872: 172953, 2020.
12. Våtsveen TK, Myhre MR, Steen CB, Wälchli S, Lingjærde OC, Bai B, Dillard P, Theodossiou TA, Holien T, Sundan A, *et al*: Artesunate shows potent anti-tumor activity in B-cell lymphoma. J Hematol Oncol 11: 23, 2018.
13. Song Q, Peng S, Che F and Zhu X: Artesunate induces ferroptosis via modulation of p38 and ERK signaling pathway in glioblastoma cells. J Pharmacol Sci 148: 300-306, 2022.
14. Markowitsch SD, Schupp P, Lauckner J, Vakhrusheva O, Slade KS, Mager R, Efferth T, Haferkamp A and Juengel E: Artesunate inhibits growth of sunitinib-resistant renal cell carcinoma cells through cell cycle arrest and induction of ferroptosis. Cancers (Basel) 12: 3150, 2020.
15. Zhang ZY, Yu SQ, Miao LY, Huang XY, Zhang XP, Zhu YP, Xia XH and Li DQ: Artesunate combined with vinorelbine plus cisplatin in treatment of advanced non-small cell lung cancer: A randomized controlled trial. Zhong Xi Yi Jie He Xue Bao 6: 134-138, 2008 (In Chinese).
16. Trimble CL, Levinson K, Maldonado L, Donovan MJ, Clark KT, Fu J, Shay ME, Sauter ME, Sanders SA, Frantz PS and Plesa M: A first-in-human proof-of-concept trial of intravaginal artesunate to treat cervical intraepithelial neoplasia 2/3 (CIN2/3). Gynecol Oncol 157: 188-194, 2020.
17. von Hagens C, Walter-Sack I, Goeckenjan M, Storch-Hagenlocher B, Sertel S, Elsässer M, Remppis BA, Munzinger J, Edler L, Efferth T, *et al*: Long-term add-on therapy (compassionate use) with oral artesunate in patients with metastatic breast cancer after participating in a phase I study (ARTIC M33/2). Phytomedicine 54: 140-148, 2019.
18. Krishna S, Ganapathi S, Ster IC, Saeed ME, Cowan M, Finlayson C, Kovacsevics H, Jansen H, Kremsner PG, Efferth T and Kumar D: A randomised, double blind, placebo-controlled pilot study of oral artesunate therapy for colorectal cancer. EBioMedicine 2: 82-90, 2014.
19. Tang W, Chen Z, Zhang W, Cheng Y, Zhang B, Wu F, Wang Q, Wang S, Rong D, Reiter FP, *et al*: The mechanisms of sorafenib resistance in hepatocellular carcinoma: Theoretical basis and therapeutic aspects. Signal Transduct Target Ther 5: 87, 2020.
20. Ravandi F, Alattar ML, Grunwald MR, Rudek MA, Rajkhowa T, Richie MA, Pierce S, Daver N, Garcia-Manero G and Faderl S: Phase 2 study of azacytidine plus sorafenib in patients with acute myeloid leukemia and FLT-3 internal tandem duplication mutation. Blood 121: 4655-4662, 2013.
21. Gibson JF, Foss F, Cooper D, Seropian S, Irizarry D, Barbarotta L and Lansigan F: Pilot study of sorafenib in relapsed or refractory peripheral and cutaneous T-cell lymphoma. Br J Haematol 167: 141-144, 2014.
22. Kießling MK, Nicolay JP, Schlör T, Klemke CD, Süss D, Krammer PH and Gülow K: NRAS mutations in cutaneous T cell lymphoma (CTCL) sensitize tumors towards treatment with the multikinase inhibitor sorafenib. Oncotarget 8: 45687-45697, 2017.
23. Hamed HA, Tavallai S, Grant S, Poklepovic A and Dent P: Sorafenib/regorafenib and lapatinib interact to kill CNS tumor cells. J Cell Physiol 230: 131-139, 2015
24. Chen Y, Wang F, Wu P, Gong S, Gao J, Tao H, Shen Q, Wang S, Zhou Z and Jia Y: Artesunate induces apoptosis, autophagy and ferroptosis in diffuse large B cell lymphoma cells by impairing STAT3 signaling. Cell Signal 88: 110167, 2021.
25. Efferth T: From ancient herb to modern drug: Artemisia annua and artemisinin for cancer therapy. Semin Cancer Biol 46: 65-83, 2017.
26. Ruwizhi N, Maseko RB and Aderibigbe BA: Recent advances in the therapeutic efficacy of artesunate. Pharmaceutics 14: 504, 2022.
27. Zhao KC and Song ZY: Distribution and excretion of artesunate in rats. Proc Chin Acad Med Sci Peking Union Med Coll 4: 186-188, 1989.
28. Clavreul A, Roger E, Pourbaghi-Masouleh M, Lemaire L, Tétaud C and Menei P: Development and characterization of sorafenib-loaded lipid nanocapsules for the treatment of glioblastoma. Drug Deliv 25: 1756-1765, 2018.
29. Feng FB and Qiu HY: Effects of artesunate on chondrocyte proliferation, apoptosis and autophagy through the PI3K/AKT/mTOR signaling pathway in rat models with rheumatoid arthritis. Biomed Pharmacother 102: 1209-1220, 2018.
30. Thomé MP, Filippi-Chiela EC, Villodre ES, Migliavaca CB, Onzi GR, Felipe KB and Lenz G: Ratiometric analysis of acridine orange staining in the study of acidic organelles and autophagy. J Cell Sci 129: 4622-4632, 2016.
31. Su Y, Zhao B, Zhou L, Zhang Z, Shen Y, Lv H, AlQudsy LHH and Shang P: Ferroptosis, a novel pharmacological mechanism of anti-cancer drugs. Cancer Lett 483: 127-136, 2020.
32. Zhang W, Gong M, Zhang W, Mo J, Zhang S, Zhu Z, Wang X, Zhang B, Qian W, Wu Z, *et al*: Thiostrepton induces ferroptosis in pancreatic cancer cells through STAT3/GPX4 signalling. Cell Death Dis 13: 630, 2022.
33. Schmitt A, Xu W, Bucher P, Grimm M, Konantz M, Horn H, Zapukhlyak M, Berning P, Brändle M, Jarboui MA, *et al*: Dimethyl fumarate induces ferroptosis and impairs NF-κB/STAT3 signaling in DLBCL. Blood 138: 871-884, 2021.
34. Zhao X, Guo X, Yue W, Wang J, Yang J and Chen J: Artemether suppresses cell proliferation and induces apoptosis in diffuse large B cell lymphoma cells. Exp Ther Med 14: 4083-4090, 2017.
35. Cheng C, Wang T, Song Z, Peng L, Gao M, Hermine O, Rousseaux S, Khochbin S, Mi JQ and Wang J: Induction of autophagy and autophagy-dependent apoptosis in diffuse large B-cell lymphoma by a new antimalarial artemisinin derivative, SM1044. Cancer Med 7: 380-396, 2018.
36. Wang N, Zeng GZ, Yin JL and Bian ZX: Artesunate activates the ATF4-CHOP-CHAC1 pathway and affects ferroptosis in burkitt's lymphoma. Biochem Biophys Res Commun 519: 533-539, 2019.
37. Xargay-Torrent S, López-Guerra M, Montraveta A, Saborit-Villarroya I, Rosich L, Navarro A, Pérez-Galán P, Roué G, Campo E and Colomer D: Sorafenib inhibits cell migration and stroma-mediated bortezomib resistance by interfering B-cell receptor signaling and protein translation in mantle cell lymphoma. Clin Cancer Res 19: 586-597, 2013.

38. Locatelli SL, Cleris L, Stirparo GG, Tartari S, Saba E, Pierdominici M, Malorni W, Carbone A, Anichini A and Carlo-Stella C: BIM upregulation and ROS-dependent necroptosis mediate the antitumor effects of the HDACi givinostat and sorafenib in hodgkin lymphoma cell line xenografts. Leukemia 28: 1861-1871, 2014.
39. Carlo-Stella C, Locatelli SL, Giacomini A, Cleris L, Saba E, Righi M, Guidetti A and Gianni AM: Sorafenib inhibits lymphoma xenografts by targeting MAPK/ERK and AKT pathways in tumor and vascular cells. PLoS One 8: e61603, 2013.
40. Ramakrishnan V, Timm M, Haug JL, Kimlinger TK, Halling T, Wellik LE, Witzig TE, Rajkumar SV, Adjei AA and Kumar S: Sorafenib, a multikinase inhibitor, is effective in vitro against non-Hodgkin lymphoma and synergizes with the mTOR inhibitor rapamycin. Am J Hematol 87: 277-283, 2012.
41. Locatelli SL, Giacomini A, Guidetti A, Cleris L, Mortarini R, Anichini A, Gianni AM and Carlo-Stella C: Perifosine and sorafenib combination induces mitochondrial cell death and antitumor effects in NOD/SCID mice with Hodgkin lymphoma cell line xenografts. Leukemia 27: 1677-1687, 2013.
42. Takashima Y, Hayano A and Yamanaka R: Metabolome analysis reveals excessive glycolysis via PI3K/AKT/mTOR and RAS/MAPK signaling in methotrexate-resistant primary CNS lymphoma-derived cells. Clin Cancer Res 26: 2754-2766, 2020.
43. Jiang F, Zhou JY, Zhang D, Liu MH and Chen YG: Artesunate induces apoptosis and autophagy in HCT116 colon cancer cells, and autophagy inhibition enhances the artesunateinduced apoptosis. Int J Mol Med 42: 1295-1304, 2018.
44. Zhou X, Chen Y, Wang F, Wu H, Zhang Y, Liu J, Cai Y, Huang S, He N, Hu Z and Jin X: Artesunate induces autophagy dependent apoptosis through upregulating ROS and activating AMPK-mTOR-ULK1 axis in human bladder cancer cells. Chem Biol Interact 331: 109273, 2020.
45. Shimizu S, Takehara T, Hikita H, Kodama T, Tsunematsu H, Miyagi T, Hosui A, Ishida H, Tatsumi T, Kanto T, *et al*: Inhibition of autophagy potentiates the antitumor effect of the multikinase inhibitor sorafenib in hepatocellular carcinoma. Int J Cancer 131: 548-557, 2012.
46. Heqing Y, Bin L, Xuemei Y and Linfa L: The role and mechanism of autophagy in sorafenib targeted cancer therapy. Crit Rev Oncol Hematol 100: 137-140, 2016.
47. Liang C, Zhang X, Yang M and Dong X: Recent progress in ferroptosis inducers for cancer therapy. Adv Mater 31: e1904197, 2019.
48. Hassannia B, Vandenabeele P and Vanden Berghe T: Targeting ferroptosis to iron out cancer. Cancer Cell 35: 830-849, 2019.
49. Mou Y, Wang J, Wu J, He D, Zhang C, Duan C and Li B: Ferroptosis, a new form of cell death: Opportunities and challenges in cancer. J Hematol Oncol 12: 34, 2019.
50. Yang WS, SriRamaratnam R, Welsch ME, Shimada K, Skouta R, Viswanathan VS, Cheah JH, Clemons PA, Shamji AF, Clish CB, *et al*: Regulation of ferroptotic cancer cell death by GPX4. Cell 156: 317-331, 2014.
51. Li J, Cao F, Yin HL, Huang ZJ, Lin ZT, Mao N, Sun B and Wang G: Ferroptosis: Past, present and future. Cell Death Dis 11: 88, 2020.
52. Zhang Y, Tan H, Daniels JD, Zandkarimi F, Liu H, Brown LM, Uchida K, O'Connor OA and Stockwell BR: Imidazole ketone erastin induces ferroptosis and slows tumor growth in a mouse lymphoma model. Cell Chem Biol 26: 623-633.e9, 2019.
53. Tang D, Tang D, Kang R, Berghe TV, Vandenabeele P and Kroemer G: The molecular machinery of regulated cell death. Cell Res 29: 347-364, 2019.
54. Galluzzi L, Vitale I, Aaronson SA, Abrams JM, Adam D, Agostinis P, Alnemri ES, Altucci L, Amelio I, Andrews DW, *et al*: Molecular mechanisms of cell death: Recommendations of the nomenclature committee on cell death 2018. Cell Death Differ 25: 486-541, 2018.
55. Lee Y, Lee DH, Choudry HA, Bartlett DL and Lee YJ: Ferroptosis-induced endoplasmic reticulum stress: Cross-talk between ferroptosis and apoptosis. Mol Cancer Res 16: 1073-1076, 2018.
56. Zhu F, Wang KB and Rui L: STAT3 activation and oncogenesis in lymphoma. Cancers (Basel) 12: 19, 2019.
57. Lobello C, Tichy B, Bystry V, Radova L, Filip D, Mraz M, Montes-Mojarro IA, Prokoph N, Larose H and Liang HC: STAT3 and TP53 mutations associate with poor prognosis in anaplastic large cell lymphoma. Leukemia 35: 1500-1505, 2021.